2024 International Conference on Unmanned Aircraft Systems (ICUAS)
June 4-7, 2024. Chania, Crete, Greece

Enhancing traffic state estimation using UAV-based measurements

Y. Englezou, S. Timotheou and C.G. Panayiotou

Abstract— **Traffic state estimation is a challenging task due to the collection of sparse and noisy measurements from specific points of the traffic network. The emergence of Unmanned Aerial Vehicles (UAVs) provides new capabilities for traffic state estimation using density measurements at irregular time-points from all links of a given network under study. This work proposes a data-driven traffic density estimation method utilising measurements collected from a swarm of UAVs deployed over the network under study and no traffic models or historical data are required. A simulation study is conducted to compare the quality of information obtained from UAV-based measurements, to the information provided by other sensing technologies, particularly fixed-location sensors and Connected and Automated Vehicles (CAVs). Notably, while CAV-based and UAV-based sensing provide information with higher spatiotemporal resolutions compared to fixed-location sensors, UAV-based sensing exhibits higher estimation accuracy even under low penetration rates of UAVs flying above the network and low percentages of network coverage.**

I. Introduction

Traffic state estimation (TSE) is one of the major tools in transportation monitoring as it helps road operators in decision-making and the implementation of various control strategies, and involves deriving traffic variables from a set of noisy observed traffic measurements on specific road segments. This procedure relies on the chosen estimation methodology, the traffic flow models employed to characterise traffic dynamics, and the available traffic data. Typically, TSE tasks require data collected using either fixed-location sensors, termed *fixed-location sensor data* [1], or probe sensors (e.g., GPS, smartphones, connected vehicles) mounted on vehicles, termed *Floating Car Data (FCD)* [2].

Stationary or fixed-location data, provide information on traffic state variables (e.g. flow and time occupancy) collected by stationary sensors (e.g. loop detectors, cameras) at their installed locations. The estimation capabilities using such data are often limited, as stationary sensors record information only at specific locations [3]. Fixed-location sensors have been widely used on highways and urban networks since the early 1990s [4], due to their widespread availability [5]. However, they come with limitations including sparse deployment [1], high installation costs [6], and the inability to measure traffic parameters beyond their location [7].

Mobile data, i.e. data collected by mobile sensors (on-vehicle GPS, lidars), referred to as Floating Car Data (FCD), has become a promising source of traffic measurements from a wider spatiotemporal domain. FCD provides a broader spatiotemporal perspective as vehicles continuously collect data while in motion [8], significantly enhancing TSE. However, FCD raise security and privacy issues as they continuously disseminate the location of travellers and offer state information only at certain parts of the network [9].

Connected and Automated Vehicles (CAVs) introduce innovative capabilities for enhanced traffic sensing. These vehicles gather extensive data about their surroundings, capturing information like spacing between neighbouring vehicles to derive the traffic density. This data is termed extended Floating Car Data (xFCD). Researchers have investigated the potential of CAVs to estimate vital traffic variables and share traffic information with nearby vehicles [10]. One such approach utilises a streaming-data-driven method to estimate traffic density on highways based on Edie's definitions, using only xFCD [11]. A fully Bayesian data-driven approach for TSE in multi-lane highways was introduced, relying solely on xFCD, showcasing high-quality estimation results even at low penetration rates of CAVs [12]. However, CAVs face privacy concerns as they continuously record a vehicle's position [13], while they can only provide traffic data within their specific route and time frame under study [14].

Unmanned Aerial Vehicles (UAVs) are considered a promising technology for a variety of transportation-related applications. UAVs can be equipped with several imaging devices including day and night video cameras, infrared cameras, laser scanners, road weather systems and can be used for many transportation-related operations; estimate OD matrices, monitor freeway conditions and track vehicle movements at intersections [15]. Research regarding traffic monitoring using UAVs has focused on how to remotely capture traffic information above the ground [16]. The collected information is then used for surveillance, managing traffic congestion and road safety, optimising traffic signals, highway infrastructure management and inferring traffic parameters [17]. Despite the extensive body of literature on traffic management, there is a gap on the main monitoring tasks (i.e. TSE, OD matrix estimation) using measurements obtained from UAVs. The only attempt is a recent study that investigated the impact on UAV-based traffic sensing on OD matrix estimation illustrating significantly better performance compared to sparse stationary measurements, even when the number of measurements per time step with the UAVs is smaller [18]. Furthermore, UAVs have been used to develop

This work is supported by the European Union (i. ERC, URANUS, No. 101088124 and, ii. Horizon 2020 Teaming, KIOS CoE, No. 739551), and the Government of the Republic of Cyprus through the Deputy Ministry of Research, Innovation, and Digital Strategy. Views and opinions expressed are however those of the author(s) only and do not necessarily reflect those of the European Union or the European Research Council Executive Agency. Neither the European Union nor the granting authority can be held responsible for them.

Y. Englezou, S. Timotheou and C. G. Panayiotou are with the KIOS Research and Innovation Center of Excellence, and the Department of Electrical and Computer Engineering, University of Cyprus, {englezou.yiolanda, timotheou.stelios, christosp}@ucy.ac.cy

2024 International Conference on Unmanned Aircraft Systems (ICUAS) | 979-8-3503-5788-2/24/$31.00 ©2024 IEEE | DOI: 10.1109/ICUAS60882.2024.10556942

high resolution datasets that provide detailed information about vehicle trajectories [19].

The contributions of this work are as follows. We present a traffic density estimation approach using only streaming-data-driven measurements from UAV-based sensing. This approach capitalises the unique advantages offered by UAVs, to enhance TSE tasks. Towards this, we employ a Bayesian framework using a Gaussian process model [20], that provides fine-grained traffic density estimations, as well as probability bounds of the estimated values. We aim to generate fine-grained *virtual measurements*, i.e. measurements that have not been directly observed, along with their quantified uncertainty. In contrast with other works in the literature, we aim to derive traffic density estimations using only streaming-data-driven measurements, without reliance on historical data or a specific traffic model. To assess the efficacy of UAV-based sensing, we conduct a comparative analysis with traffic density estimations derived from measurements obtained by fixed-location sensors and CAVs. This investigation not only enhances methodologies for traffic density estimation, but also sheds light on the relative strengths and limitations of different sensing technologies in urban environments. Such insights are crucial for informing future urban management strategies.

In the next section we formulate the traffic density estimation problem for the three different types of measurements. In Section III, we describe the Gaussian process model tailored to the estimation of traffic density and the Bayesian streaming-data-driven framework for the solution of the traffic density estimation problem. In Section IV we present a simulation study that is performed to evaluate the proposed estimation methodology using measurements from three different sensing technologies. Last, Section V summarises and outlines the main outcomes of this work.

II. Problem Formulation

Assume a traffic network with N^E distinct road segments with each segment consisting of N^L distinct road lanes. The network under study is monitored for the total fixed time period T. Let $\mathcal{M}_\tau$ be the set of monitored segments at time-point τ. The number of monitored segments at time-point τ^{sense}, sense $= \{\text{fixed}, \text{CAV}, \text{UAV}\}$[1], is denoted by $N^\tau = |\mathcal{M}_\tau|$, such that $N^\tau \leq N^E$. We aim to derive traffic density estimations for distinct road segments over T. The traffic density is estimated for fixed time-window durations denoted by T^W, such that $N^W = T/T^W$ different density values are obtained in T, with $\mathcal{N}^W = \{1, \ldots, N^W\}$. Density measurements are obtained for discrete but not necessarily continuous time-points.

A time-space region $\mathcal{A}_{ij}$ is defined through a space region $\mathcal{R}_i = \{x | x_{i-1} \leq x \leq x_i\}$, $i \in \mathcal{N}^E$, and a time-window $\mathcal{T}_j = \{\tau | \tau_{j-1} \leq \tau \leq \tau_j\}$, $j \in \mathcal{N}^W$. The true traffic density, ρ^{true}, in a specific time-space region $\mathcal{A}_{ij}$ is computed according to Edie's definition [21] as

$$\rho^{true} = \frac{t(\mathcal{A}_{ij})}{|\mathcal{A}_{ij}|}, \tag{1}$$

where $t(\mathcal{A}_{ij})$ is the total time-spent of all vehicles in $\mathcal{A}_{ij}$ and $|\mathcal{A}_{ij}|$ is the time-space area of region $\mathcal{A}_{ij}$. Following, we formulate the traffic density estimation problem with respect to the available measurements in the network under study, and define the time-space region with respect to UAVs.

Because the analysis is uniform across all time-space regions, we drop indices i, j in the remainder of this work.

A. UAV-based measurements

We consider N^U UAVs flying above the network under study, with $\mathcal{N}^U$ the set of all UAVs, such that $N^U = |\mathcal{N}^U|$. For simplicity we assume that all UAVs have identical flying and sensing capabilities. We discretise the network under study into S^U UAV sampling points, where $\mathcal{S}^U = \{1, \ldots, S^U\}$ the set of all sampling points. UAVs hover above the network at height h^U [m]. A UAV camera has field of view $90°$, meaning that the UAV has circular line-of-sight with radius R [m] and $R = h^U$. For the purposes of this work we assume that each road segment is fully monitored from a specific sampling point.

Each UAV traverses between sampling points with constant speed v^{UAV} [m/s] and requires $T^U = d_{ss'}/v^{UAV}$ [s] to traverse between neighbouring sampling points, where $d_{ss'}$ is the distance between sampling points x_s and $x_{s'}$, $s, s' \in \mathcal{S}^U$. Let T^H [s] be the hovering duration of a UAV above a given sampling point. We assume that each UAV records measurements only for the hovering time, T^H [s], above each sampling point, whereas no measurements are recorded during T^U.

UAVs are equipped with cameras and have computer vision capabilities for measuring vehicle speed, position, acceleration, etc., as well as road link density and flow. We define as $\mathcal{N}^D$ the set of all vehicles that are within the line-of-sight of any UAV in time-space region $\mathcal{A}$. Hence the traffic density of $\mathcal{A}$ is given as

$$\rho^{UAV} = \frac{\sum_{d \in \mathcal{N}^D} t_d}{\sum_{d \in \mathcal{N}^D} a_d}, \tag{2}$$

where a_d, $d \in \mathcal{N}^D$, is the area of the time-space region between a vehicle and its leading vehicle, and t_d is the time-spent of vehicle d in region $\mathcal{A}$, within the line-of-sight of any UAV.

At different sampling points, UAVs can observe specific subsets of the network, such that multiple UAVs observe potentially overlapping subsets of time-space region $\mathcal{A}$. Consolidating these time-space subsets from different UAVs yields the following measurements:

- The *density* of road segment i calculated using Equation (2), given as $\boldsymbol{\rho}_i^{UAV} = [\rho_{i,1}^{UAV}, \ldots, \rho_{i,L_i'}^{UAV}]^{\mathrm{T}}$ [veh/km].
- The time-window indices associated with density measurements, given as $\boldsymbol{\tau}_i^{UAV} = [\tau_{i,1}^{UAV}, \ldots, \tau_{i,L_i'}^{UAV}]^{\mathrm{T}}$ [s].

Above, $\rho_{i,l}^{UAV}$ is the lth measurement obtained for road segment i, $\tau_{i,l}^{UAV} = j'$ indicates that the lth measurement

[1]The time-points may differ for each sensing technology used to monitor specific segments of the traffic network under study.

corresponds to time-window $\mathcal{T}_{j'}$ and L'_i is the total number of measurements in the specific road segment. The absence of index $\hat{j}$ in $\boldsymbol{\tau}_i^{UAV}$ indicates that no UAV has observed any part of road segment i over time-window $\mathcal{T}_{\hat{j}}$.

To evaluate the quality of information obtained by UAVs, in the next two sections we formulate the traffic density estimation problem with respect to two additional sensing technologies, namely fixed-location sensors (Section II-B) and CAVs (Section II-C).

B. Fixed-location sensor measurements

Assume that fixed-location sensors are deployed on specific road segments, i.e. monitored segments, in a traffic network such that they measure the traffic density in different time-windows. Traditionally, fixed-location sensors observe the traffic continuously at their installed location and report vehicle counts and occupancy, from which estimates of the traffic density for each lane can be obtained, subject to some uncertainty. In this work, we utilise Edie's definition of traffic density (1) and obtain density measurements through the vehicle trajectory time-space diagram. The time-window duration T^W is the aggregation time-unit of the measurements such that we seek to find a new traffic density estimation every T^W, yielding the following data:

- The *traffic density* of road segment i, given as $\boldsymbol{\rho}_i^{fixed} = [\rho_{i,1}^{fixed}, \dots, \rho_{i,N^W}^{fixed}]^{\mathrm{T}}$ [veh/km].

Above, N^W is the total number of measurements obtained in time, equal to the number of all time-windows $\mathcal{T}_j$, $j \in \mathcal{N}^W$. Without loss of generality, we assume that the measured density at the fixed point of the road segment is constant across the whole segment. Note that the set of monitored segments remains fixed over time and no information is provided for road segments with no sensor.

C. CAV-based measurements

In the traffic network under study, we assume that there are two types of vehicles: CAVs with the ability to measure the distance to their leading vehicle, and Human-Driven Vehicles (HDVs) without this measuring capability. We denote as $\mathcal{N}^V$ the set of all vehicles and $\mathcal{N}^C$ the set of CAVs in a given time-space region $\mathcal{A}$, with $\mathcal{N}^C \subseteq \mathcal{N}^V$, and $N^V = |\mathcal{N}^V|$, $N^C = |\mathcal{N}^C|$. Each CAV $c \in \mathcal{N}^C$ in $\mathcal{A}$ records the following measurements every $T^S \ll T^W$ time units:

- The *speed* $\mathbf{u}_c = [u_{c,1}, \dots, u_{c,M_c}]^{\mathrm{T}}$ [km/h].
- The *time spent* of CAV $c \in \mathcal{N}^C$ in the specific region $\mathcal{A}$, is approximately given by $t_c = \hat{\tau}_{c,M_c} - \hat{\tau}_{c,1}$ [h], where $\hat{\tau}_{c,M_c}$ and $\hat{\tau}_{c,1}$ are the time recordings of the last and first measurements of the CAV, respectively.
- The *area* of the time-space region between CAV $c \in \mathcal{N}^C$ and its leading vehicle in region $\mathcal{A}$, denoted as $a_c = \mathcal{A} \cap \mathcal{S}_c$ [km×h]. By using the position and the distance between the front-bumper of the ego vehicle and the rear-bumper of its leading vehicle, we derive $\mathcal{S}_c$, the time-space region between CAV c and its leading vehicle. Finally, we calculate a_c, which is the value of the intersecting area between $\mathcal{A}$ and $\mathcal{S}_c$.

For CAV-based measurements, the true traffic density, ρ^{true}, in a specific time-space region can be re-written as

$$\rho^{true} = \frac{\sum_{n \in \mathcal{N}^V} t_n}{\sum_{n \in \mathcal{N}^V} a_n}, \tag{3}$$

which indicates that if all vehicles in the specific road segment are CAVs then the traffic density is known. However only a subset of vehicles in the network are CAVs hence Equation (3) becomes

$$\rho^{CAV} = \frac{\sum_{c \in \mathcal{N}^C} t_c}{\sum_{c \in \mathcal{N}^C} a_c}, \tag{4}$$

indicating the traffic density in a specific time-space region.

Without loss of generality, we assume that each road segment in the network is a distinct time-space region. Given that a penetration rate of CAVs is deployed in the network under study, the measurements provided by CAVs, $\mathbf{u}_c$, t_c and a_c, $\forall c \in \mathcal{N}^C$, yield the following data:

- The *traffic density* of road segment i calculated using Equation (4), given as $\boldsymbol{\rho}_i^{CAV} = [\rho_{i,1}^{CAV}, \dots, \rho_{i,L_i}^{CAV}]^{\mathrm{T}}$ [veh/km].
- The time-window indices associated with the traffic density measurements, given as $\boldsymbol{\tau}_i^{CAV} = [\tau_{i,1}^{CAV}, \dots, \tau_{i,L_i}^{CAV}]$.

As before, $\rho_{i,l}^{CAV}$ is the lth density measurement obtained for road segment i; $\tau_{i,l}^{CAV}$ denotes the index of the time-window of the lth density measurement such that $\tau_{i,l}^{CAV} = j'$ indicates that the lth measurement corresponds to time-window $\mathcal{T}_{j'}$. In addition, L_i gives the total number of measurements for the specific road segment. The absence of index $\hat{j}$ in $\boldsymbol{\tau}_i^{CAV}$ indicates that no CAV has observed any part of road segment i over time-window $\mathcal{T}_{\hat{j}}$.

III. Solution Approach

The measurements obtained from the three different sensing technologies, i.e. fixed-location sensors, CAVs and UAVs differ in terms of their frequency obtained, while the set of measured links varies at each time-step. First, fixed-location sensors provide density measurements at equally spaced time-points in $\mathcal{T}$, while the set of measured links remains constant over time. Second, CAV-based measurements provide traffic density measurements of segment i at irregular points, the accuracy of traffic density measurements depends on the penetration rate of CAVs deployed in the network [11], and the set of measured links changes at each time-point according to the position of the CAVs. Last, similar to the CAV-based measurements, UAV-based measurements are not continuous with respect to different time-points and the set of measured links changes at each time-point according to the sampling position of the set of UAVs.

A. Gaussian process model

Given data of the form $(\boldsymbol{\rho}_i, \boldsymbol{\tau}_i)$ where $\boldsymbol{\tau}_i \in \mathbb{Z}_+^{L_i}$, and $\boldsymbol{\rho}_i$ the vector of measured traffic densities of segment $i \in \mathcal{M}_\tau$, at irregular sampling time-points $\boldsymbol{\tau}_i$, we assume that

$$\boldsymbol{\rho}_i = g(\boldsymbol{\tau}_i) + \boldsymbol{\varepsilon}_i, \tag{5}$$

where function $g(\cdot)$ is unknown and each $\boldsymbol{\varepsilon}_i$ is the measurement noise with $\boldsymbol{\varepsilon}_i \sim N(\mathbf{0}, \sigma^2_{i,\varepsilon}\mathbf{I})$ independently. Measurement error may exist at sampled points as computer vision algorithms do not necessarily provide perfect measurements. Each measured segment $i \in \mathcal{M}_\tau$ is considered independently and one GP model will be considered for each road segment. Hence for simplicity, we hereafter drop subscript i.

A GP model is fully defined by its mean and variance function. We assume the GP prior

$$g(\boldsymbol{\tau}) \sim \text{GP}\left[\mathbf{f}^{\text{T}}(\boldsymbol{\tau})\boldsymbol{\beta}, \sigma^2\kappa(\boldsymbol{\tau}, \boldsymbol{\tau}'; \phi)\right], \tag{6}$$

where $\mathbf{f}(\boldsymbol{\tau}) = [f_0(\boldsymbol{\tau}), f_1(\boldsymbol{\tau}), \ldots, f_{q-1}(\boldsymbol{\tau})]^{\text{T}}$ is a q-vector of known regression functions, $\boldsymbol{\beta} = (\beta_0, \beta_1, \ldots\ \ldots, \beta_{q-1})^{\text{T}} \in \mathcal{B}$ is also a q-vector which contains unknown regression coefficients, also known as trend parameters, $0 \leq \kappa(\boldsymbol{\tau}, \boldsymbol{\tau}'; \phi) \leq 1$ is the known correlation function, $\phi \in \Phi = (0, \infty)$ is the unknown correlation parameter and $\sigma^2 > 0$ is the unknown constant variance. Following [22], we select constant regression functions $\mathbf{f}(\boldsymbol{\tau})$ whose coefficients, $\boldsymbol{\beta}$ are to be inferred from the data. Under prior (6), any finite collection of function evaluations $\mathbf{g} = [g(\tau_1), \ldots, g(\tau_L)]^{\text{T}}$ has a multivariate normal distribution,

$$\mathbf{g} \sim \text{N}\left[\mathbf{F}\boldsymbol{\beta}, \sigma^2\mathbf{K}(\phi)\right], \tag{7}$$

where $\mathbf{F} = [\mathbf{f}(\tau_1)\ \mathbf{f}(\tau_2) \ldots \mathbf{f}(\tau_{L_i})]^{\text{T}}$ is the $L \times q$ model matrix and $\mathbf{K}(\phi)$ is the correlation matrix with klth entry $\mathbf{K}(\phi)_{kl} = \kappa(\tau_k, \tau_l, \phi)$, $\tau_k, \tau_l \in \mathbb{Z}_+$.

Combining (5) and (7) we get

$$\boldsymbol{\rho} \mid \boldsymbol{\beta}, \sigma^2, \phi, \nu^2 \sim \text{N}(\mathbf{F}\boldsymbol{\beta}, \sigma^2[\mathbf{K}(\phi) + \nu^2\mathbf{I}_L]),$$

where $\boldsymbol{\rho} = [\rho_1, \ldots, \rho_L]^{\text{T}}$ is the L-vector of measurements and $\mathbf{I}_L$ is the $L \times L$ identity matrix. In addition, $\nu^2 = \sigma^2_\varepsilon/\sigma^2$ is the noise-to-signal ratio. Hence, hereafter we will use the new covariance matrix $\sigma^2[\mathbf{K}(\phi) + \nu^2\mathbf{I}_L] = \sigma^2\mathbf{S}$.

The likelihood function is given by:

$$\pi(\boldsymbol{\rho}|\boldsymbol{\beta}, \sigma^2, \phi, \nu^2) = \frac{\exp\left\{\frac{1}{2\sigma^2}[(\boldsymbol{\rho} - \mathbf{F}\boldsymbol{\beta})^{\text{T}}\mathbf{S}^{-1}(\boldsymbol{\rho} - \mathbf{F}\boldsymbol{\beta})]\right\}}{(2\pi\sigma^2)^L|\mathbf{S}|^{\frac{1}{2}}}. \tag{8}$$

An important aspect of the GP model involves estimating the traffic density, denoted as $\tilde{\rho}$, at an unobserved time-point $\tilde{\tau}$. To achieve this, we formulate the predictive distribution of $\tilde{\rho}$ using the statistical model (8). We set $\boldsymbol{\psi} = [\boldsymbol{\beta}, \sigma^2, \phi, \nu^2]^{\text{T}}$ and employ standard results to obtain the subsequent conditional posterior distribution:

$$\tilde{\rho} \mid \boldsymbol{\rho}, \boldsymbol{\psi} \sim \text{N}\left(\mu(\tilde{\tau}), s^2(\tilde{\tau})\right), \tag{9a}$$

$$\mu(\tilde{\tau}) = \mathbf{f}(\tilde{\tau})^{\text{T}}\boldsymbol{\beta} + \mathbf{k}(\tilde{\tau})^{\text{T}}\mathbf{S}^{-1}\left[\boldsymbol{\rho} - \mathbf{F}\boldsymbol{\beta}\right], \tag{9b}$$

$$s^2(\tilde{\tau}) = \sigma^2[(1 + \nu^2) - \mathbf{k}(\tilde{\tau})^{\text{T}}\mathbf{S}^{-1}\mathbf{k}(\tilde{\tau})]. \tag{9c}$$

Here, $\mathbf{k}(\tilde{\tau}) = [\kappa(\tilde{\tau}, \tau_1; \phi), \ldots, \kappa(\tilde{\tau}, \tau_L; \phi)]^{\text{T}}$ is the L-vector of correlations between the traffic density at each sampling time-point $\boldsymbol{\tau}$ and the traffic density at the new $\tilde{\tau}$. Equations (9b)-(9c) show that if all parameters $\boldsymbol{\beta}$, σ^2, ϕ and ν^2 were known, the traffic density at $\tilde{\tau}$ would come from a normal distribution with known mean $\mu(\tilde{\tau})$ and variance $s^2(\tilde{\tau})$. However, these parameters are unknown and need to be integrated out to obtain the unconditional posterior distribution of the traffic density, $\pi(\tilde{\rho}|\boldsymbol{\rho})$. A natural way to represent uncertainty about unknown parameters is the Bayesian paradigm.

B. Bayesian inference

Prior distributions need to be specified for all the parameters whose values are unknown. A common approach is to assume that trend parameters and the GP variance are independent of the correlation parameter and the noise, which are also independent from each other. Hence the joint prior distribution assumed in this work is $\pi(\boldsymbol{\psi}) = \pi(\boldsymbol{\beta}, \sigma^2, \phi, \nu^2) = \pi(\boldsymbol{\beta}|\sigma^2)\pi(\sigma^2)\pi(\phi)\pi(\nu^2)$.

For $\boldsymbol{\beta}$ and σ^2, we choose conjugate prior distributions [2] and assign $\boldsymbol{\beta}|\sigma^2$ a normal distribution and σ^2 an inverse-gamma distribution, $\boldsymbol{\beta}|\sigma^2 \sim N(\boldsymbol{\beta}_0, \sigma^2\mathbf{R})$ and $\sigma^2 \sim \text{IG}(a, b)$, where $\boldsymbol{\beta}_0$ is the q-vector of known prior means, $\mathbf{R}$ is a known symmetric, positive definite $q \times q$ matrix and $a, b > 0$ are known hyperparameters. For the correlation parameter ϕ and the noise variance we assume exponential distributions, $\phi \sim \text{Exp}(\lambda_\phi)$ and $\nu^2 \sim \text{Exp}(\lambda_{\nu^2})$. In these expressions, $\lambda_\phi > 0$ and $\lambda_{\nu^2} > 0$ are known hyperparameters.

By applying Bayes' rule we can compute the posterior density of $\boldsymbol{\psi}$ denoted as

$$\pi(\boldsymbol{\psi}|\boldsymbol{\rho}) \propto \pi(\boldsymbol{\beta}|\sigma^2)\pi(\sigma^2)\pi(\phi)\pi(\nu^2)\pi(\boldsymbol{\rho}|\boldsymbol{\beta}, \sigma^2, \phi, \nu^2). \tag{10}$$

This posterior is not a standard distribution, meaning it cannot be expressed in an analytical form.

To derive the posterior predictive distribution for $\tilde{\rho}$ at a new time-point $\tilde{\tau}$, it is necessary to integrate out all the unknown parameters by considering their marginal posterior distributions. We use the conditional posterior predictive distribution $\tilde{\rho} \mid \boldsymbol{\rho}, \boldsymbol{\beta}, \sigma^2, \phi, \nu^2 \sim \text{N}\left(\mu(\tilde{\tau}), s^2(\tilde{\tau})\right)$, where $\mu(\tilde{\tau})$ and $s^2(\tilde{\tau})$ are given through Equations (9b)-(9c), and the posterior distribution $\pi(\boldsymbol{\beta}, \sigma^2, \phi, \nu^2|\boldsymbol{\rho})$ given by (10). Hence, the unconditional posterior predictive distribution, is obtained by

$$\pi(\tilde{\rho} \mid \boldsymbol{\rho}) = \int\int\int\int \pi(\tilde{\rho}|\boldsymbol{\rho}, \boldsymbol{\psi})\pi(\boldsymbol{\psi}|\boldsymbol{\rho})d\boldsymbol{\beta}\ d\sigma^2\ d\phi\ d\nu^2. \tag{11}$$

However, this integral lacks an analytical solution and necessitates numerical evaluation, often facilitated by sampling techniques based on Markov chain Monte Carlo methods [23]. For more details on the Bayesian insights to derive virtual measurements, see [20].

IV. Simulation Results

To assess the efficacy of information acquired from UAVs against other traditional sensing technologies, we conduct traffic simulations using the SUMO microscopic simulator [24] on an arterial literature network, depicted in Figure 1. This simulation scenario represents the Leicester network given in Figure 1 which consists of 34 road segments. Moreover, the number of lanes varies across segments, ranging from 2 to 3 lanes. Without loss of generality, we assume unidirectional traffic progressing. Traffic enters the network

[2] A conjugate prior yields a posterior of the same family as the prior.

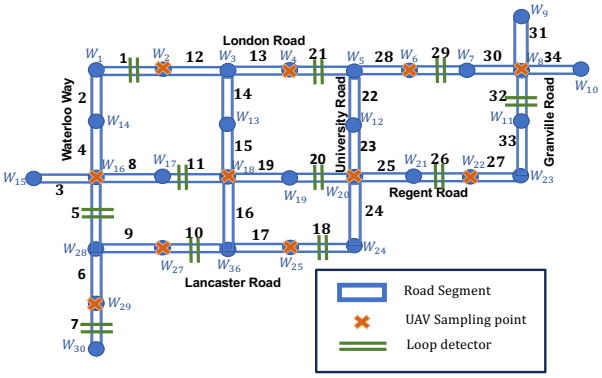

Fig. 1: An abstraction of the Leicester network, UK.

from the upstream boundary of cells 1, 2, 3 and 31 and exits from the downstream boundary of 7, 18, 24, 27, 33 and 34.

The considered scenario involves a 1.5-hour traffic simulation that initially depicts free-flow traffic conditions. Over the course of this 1.5-hour period, an accident occurs in road segment 25, prompting the closure of one lane within this segment for 30 minutes. Consequently, some upstream neighbouring road segments become congested during the 30-minute lane closure, caused by vehicles unable to exit segment 25, while downstream neighbouring road segments have a significant drop in traffic density due to the lane closure, allowing less vehicles to traverse to the next segment.

We consider three distinct sensing technologies:

(a) Fixed-location loop detectors (depicted as the green lines in Figure 1). Fixed-location sensor measurements include a traffic density measurement every 3 minutes.

(b) CAVs that measure their position, speed, and spacing every 0.2 seconds. Utilising these measurements, each connected vehicle computes and transmits its speed, $\mathbf{u}_c$, time spent, t_c, and time-space region, a_c, to an operation center, which are utilised as described in Section II-C to obtain measurements of traffic density every 3 minutes.

(c) UAVs that navigate above the road network at an average speed of $v^{UAV} = 40$ km/h. The time required for a UAV to travel between neighbouring sampling points is contingent upon their respective locations. Our assumption is that each UAV captures measurements exclusively while hovering at each sampling point, with no measurements taken while travelling between successive sampling points.

Each sensing technology is assessed under different percentages of coverage of the network under study. We define the percentage of coverage of a network (PC) as

$$\text{PC} = \frac{\text{Time-space area monitored}}{\text{Total time-space area}} 100\%.$$

For the fixed-location sensors we assume (i) 50%, (ii) 25% and (iii) 10% coverage of the network, which is defined as the percentage of road segments in the network that are equipped with fixed-location loop detectors. In addition, for the CAV-based measurements we assume 50%, 25% and 10% penetration rate of CAVs in the network, i.e. vehicles that have the capability of collecting measurements. These penetration rates can be translated to the percentages of network coverage by taking the ratio of the time-space are covered by each percentage of CAVs over the total time-space region of the whole network and time duration under study. Hence for a fair comparison among the three different sensing technologies, we have that 50% penetration rate of CAVs corresponds to 47% of network coverage, 25% penetration rate of CAVs corresponds to 23% of network coverage and 10% penetration rate of CAVs corresponds to 9% of network coverage. Last, for the UAVs we consider different deployment scenarios such as the percentage of network coverage per sampling time-point is (i) 50%, (ii) 25% and (iii) 10%. The UAV deployment scenarios assumed are as follows: (i) $N^U = 3$ with fixed trajectories i.e. 50% penetration rate, (ii) $N^U = 2$ with fixed trajectories i.e. 25% penetration rate and, (iii) $N^U = 1$ with fixed trajectory, i.e. 10% penetration rate.

We estimate the traffic density for each road segment of the network using the different sensing technologies and settings for each technology. We use the Mean Absolute Percentage Error (MAPE) between the sth estimated traffic density, $\hat{\rho}_s^{\text{sense}}$, sense $\in \{\text{fixed}, \text{CAV}, \text{UAV}\}$, and the sth true traffic density ρ_s^{true} to compare the performance of each technology given by

$$\text{MAPE} = \frac{1}{S}\sum_{s=1}^{S}\frac{|\rho_s^{true} - \hat{\rho}_s^{\text{sense}}|}{\rho_s^{true}} 100\%, \tag{12}$$

where S is the total number of estimations. The mean value of the derived probability distribution, $\pi(\tilde{\rho}|\rho)$, is calculated by drawing an independent identically distributed sample from the posterior predictive distribution using Equation (11). The MAPE is averaged across density estimations of all road segments for each distinct sensing technology and settings of each technology. In addition to the MAPE, we calculate the standard deviation (SD) of the MAPE to show the consistency of estimation across different road segments.

Initially we obtain aggregated results of the three sensing technologies by averaging the MAPE over all road segments, for different coverage percentages. To eliminate any biases we run the estimation procedure 50 times for each sensing technology, each time assuming different settings, e.g. different locations for the fixed-location sensors, choosing different vehicles to behave as CAVs during the simulation setup and different starting sampling locations of UAVs. Note that both the CAVs and UAVs are able to obtain sparse density measurements for all road segments within the total period under study, while fixed-location sensors by definition can only obtain measurements at their fixed locations. Hence for a fair comparison, we extrapolate density estimations using data from the fixed locations to neighbouring locations that are not equipped with such sensors. For this task we use kriging, a well-known spatial interpolation technique [25].

As shown in Table I for around 50% coverage of the network, i.e. seventeen fixed-location sensors, or three UAVs hovering above the network, or 50% penetration of CAVs moving within the network, all sensing technologies yield MAPE less than 20%, with fixed-location sensors and UAVs resulting in 4% less error than CAVs. As the percentage

MAPE (%) and MAPE SD (%)						
Sensing technology	**∼50% coverage**		**∼25% coverage**		**∼10% coverage**	
	MAPE	**SD**	**MAPE**	**SD**	**MAPE**	**SD**
Fixed-location sensors	15.5	12.1	33.6	32.1	58.1	22.1
UAVs	16.1	16.6	22.1	19.2	27.1	15.1
CAVs	19.7	17.1	21.5	14.5	36.3	15.9

TABLE I: Average mean absolute percentage error (MAPE) and MAPE standard deviation (SD) of all road segments for the different sensing technologies and different percentages of network coverage.

of network coverage decreases the MAPE increases for all technologies, with fixed-location sensors resulting in MAPE higher than 50% for 10% network coverage. Both UAVs and CAVs yield lower values of MAPE with UAVs having the best performance for around 10% network coverage, while for around 25% network coverage UAVs and CAVs yield similar estimation results.

Note that the estimation window of CAVs plays an important role to the estimation results. A recent paper has presented a detailed analysis of the impact of the duration of time-window, concluding that larger time-window durations yield more accurate results [12]. Further, the hovering time of a UAV above a sampling location affects the estimation accuracy of the traffic density, with small hovering duration yielding more accurate results as illustrated in [20], while both the UAVs' trajectories and the selection of UAV sampling points significantly influence the estimation process.

Following we present estimation results per road segment for each sensing technology and the different percentages of network coverage. We choose four road segments to present these results, namely road segment 11, 19, 26 and 27. This selection is done to showcase the performance of the estimation procedure both under free-flow and congested conditions. Figures 2-4 depict the per road segment estimated density for fixed-location sensors, CAVs and UAVs, respectively, for 50% network coverage. Figures 5-7 and 8-10 are the corresponding figures for 25% and 10% coverage.

In Figures 2-10, the estimated density values are the posterior medians of the GP model (blue dashed lines), along with pointwise 95% probability bounds around the estimated values (black dotted lines). In addition, black bullets correspond to the density measurements obtained/derived from each sensing technology, while the solid lines correspond to the true traffic density of the particular segment. Subfigures (a) depict the results for road segment 11, (b) for road segment 19, (c) for road segment 26 and (d) for road segment 27, as shown in Figure 1. Note that for the fixed-location sensors and segments with no sensors we only obtain an estimation of the traffic density through extrapolation of neighbouring spatial measurements using kriging.

As shown, data obtained from fixed-location sensors yield highly accurate results for road segments that are equipped with a sensor, e.g. Figures 2 (a), 2 (c), however extrapolation yields large errors especially as the percentage of network coverage becomes smaller, e.g. Figure 2 (b). CAV-based measurements yield accurate results for large penetration rates, e.g. Figure 3 (d), while estimation error becomes larger as the deployed penetration rate of CAVs becomes smaller and more specifically for large values of traffic density, e.g.

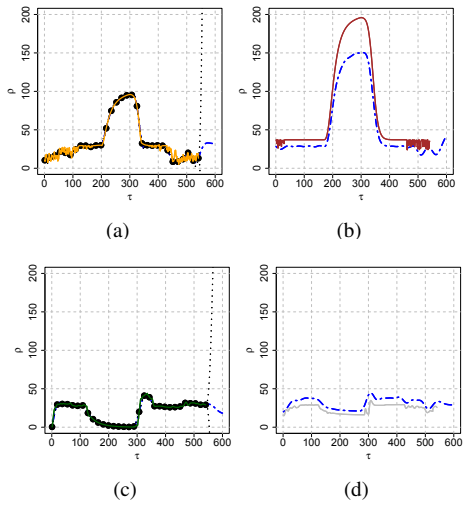

Fig. 2: Fixed-location sensors: 50% network coverage.

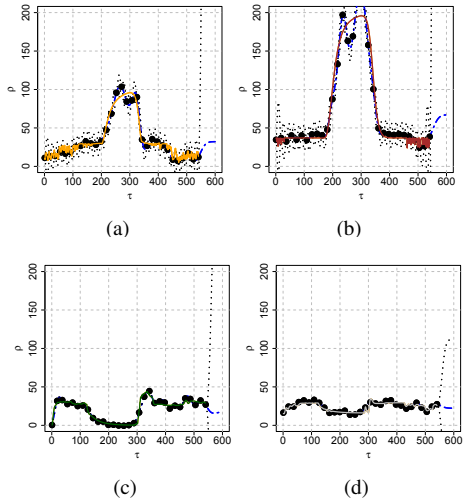

Fig. 3: CAVs: 50% penetration rate (47% network coverage).

Figures 6 (b), 9 (b). This increase in the estimation error might result from the fact that lower penetration rates of CAVs yield biased results of traffic density [11]. Similar to CAV-based measurements, UAV-based measurements yield accurate results for large network coverage, i.e. three UAVs flying above the network under study, e.g. Figures 4 (a)-(d), while estimation error becomes larger as the number of deployed UAVs becomes smaller, i.e. the network coverage percentage decreases, e.g. Figures 10 (a), 10 (b), while the effect of increased error for larger values of traffic density

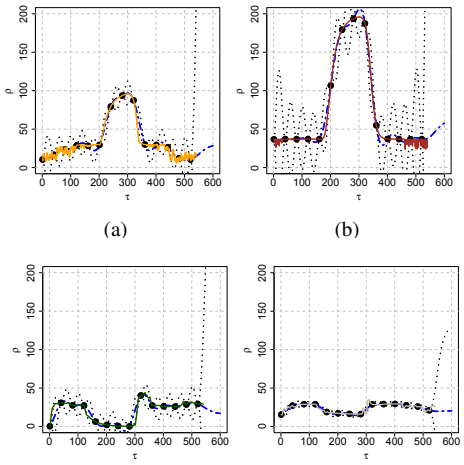

Fig. 4: UAVs: 50% network coverage.

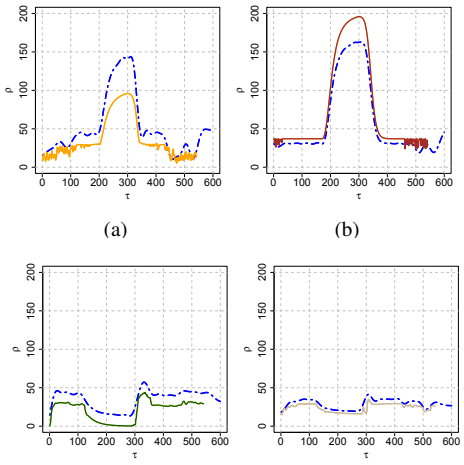

Fig. 5: Fixed-location sensors: 25% network coverage.

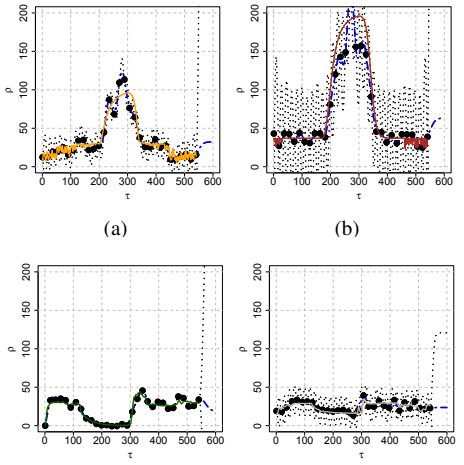

Fig. 6: CAVs: 25% penetration rate (23% network coverage).

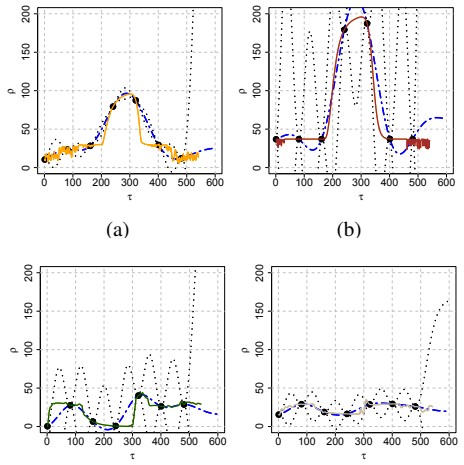

Fig. 7: UAVs: 25% network coverage.

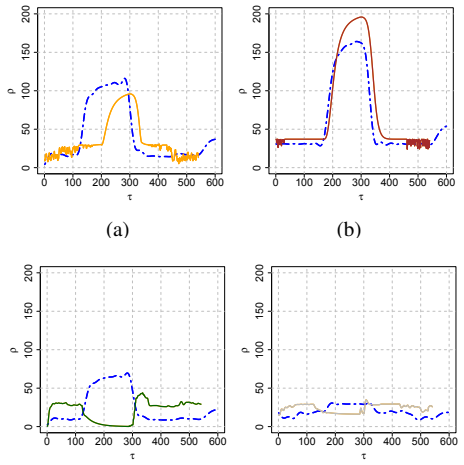

Fig. 8: Fixed-location sensors: 10% network coverage.

is not as obvious as with CAV-based measurements, as also evident in the results given in Table I.

V. Conclusions

In this work we have presented a novel streaming-data-driven probabilistic methodology, in which the Gaussian Process (GP) model is integrated with the Bayesian framework to effectively calculate traffic density estimates, even in cases where only a limited number of measurements are available within the designated time interval being examined. Information from three different sensing technologies, namely fixed-location sensors, CAVs and UAVs, is extracted through the time-space vehicle trajectory diagram.

The main conclusions of this work are: (i) fixed-location sensors deployed in the network yield highly accurate results for segments equipped with such sensors, however there exists a strong dependence between the number and location of fixed-location sensors and estimation accuracy; (ii) there exists a trade-off between the penetration rate of CAVs and estimation accuracy especially for higher values of traffic

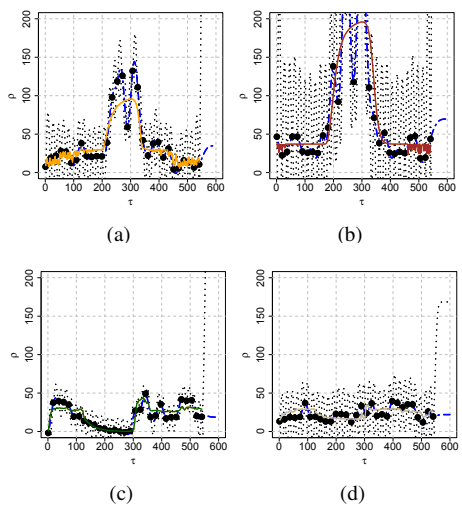

Fig. 9: CAVs: 10% penetration rate (9% network coverage).

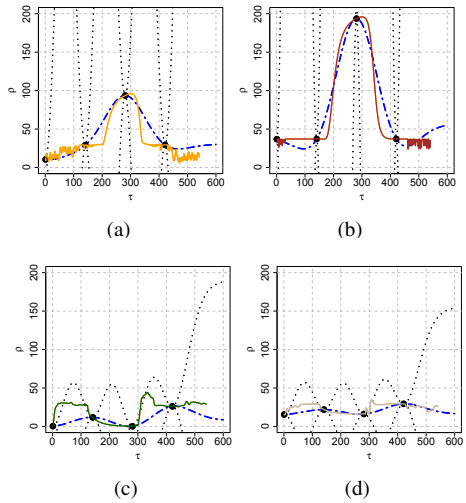

Fig. 10: UAVs: 10% network coverage.

density despite the fact that CAVs offer measurements from a higher spatiotemporal domain; (iii) UAVs yield the most accurate results among the three sensing technologies, cover high spatiotemporal resolutions of the network under study, while as the percentage of network coverage decreases the estimation error does not change significantly.

REFERENCES

[1] J. W. C. Van Lint and S. P. Hoogendoorn, "A robust and efficient method for fusing heterogeneous data from traffic sensors on freeways," *Computer-Aided Civil and Infrastructure Engineering*, vol. 25, pp. 596–612, 2010.

[2] S. Papadopoulou, S. Roncoli, N. Bekiaris-Liberis, I. Papamichail, and M. Papageorgiou, "Microscopic simulation-based validation of a per-lane traffic state estimation scheme for highways with connected vehicles," *Transportation Research Part C: Emerging Technologies*, vol. 86, pp. 441–452, 2018.

[3] T. Darwish and K. A. Bakar, "Trafc density estimation in vehicular ad hoc networks: a review," *Ad Hoc Networks*, pp. 337–351, 2015.

[4] B. D. Greenshields, "A study of traffic capacity," in *Highway Research Board Proceedings*, vol. 14, 1935, pp. 448–477.

[5] Y. Wang and M. Papageorgiou, "Real-time freeway traffic state estimation based on extended Kalman filter: A general approach," *Transportation Research Part B*, vol. 39, pp. 141–167, 2005.

[6] T. Darwish and K. A. Bakar, "Traffic density estimation in vehicular ad hoc networks: A review." *Ad Hoc Networks*, vol. 24, pp. 337–351, 2015.

[7] B. Coifman, "Revisiting the empirical fundamental relationship," *Transportation Research Part B*, vol. 68, pp. 173–184, 2014.

[8] J. C. Herrera, D. B. Work, R. Herring, X. J. Ban, Q. Jacobson, and A. M. Bayen, "Evaluation of traffic data obtained via GPS-enabled mobile phones: the mobile century field experiment," *Transportation Research Part C*, vol. 18, pp. 568–583, 2010.

[9] D. F. Llorca, M. A. Sotelo, S. Sánchez, M. Ocaña, J. M. Rodríguez-Ascariz, and M. A. García-Garrido, "Traffic data collection for floating car data enhancement in v2i networks," *EURASIP Journal on Advances in Signal Processing*, vol. 2010, p. 719294, 2010.

[10] Y. Ma, M. Chowdhury, A. Sadek, and M. Jeihani, "Real-time highway traffic condition assessment framework using vehicle-infrastructure integration (vii) with artificial intelligence (ai)," *IEEE Transactions on Intelligent Transportation Systems*, vol. 10, pp. 615–627, 2010.

[11] T. Seo, T. Kusakabe, and Y. Asakura, "Estimation of flow and density using probe vehicles with spacing measurement equipment," *Transportation Research Part C*, vol. 53, pp. 134–150, 2015.

[12] V. Kyriacou, Y. Englezou, C. Panayiotou, and S. Timotheou, "Bayesian traffic state estimation using extended floating car data," *IEEE Transactions on Intelligent Transportation Systems*, vol. 24, pp. 1518–1532, 2022.

[13] D. F. Llorca, M. A. Satelo, S. Sánchez, M. O. na, J. M. Rodríguez-Ascariz, and M. A. Garcìa-Garrido, "Traffic data collection for floating car data enhancement in v2i networks," *EURASIP Journal of Advanced Signal Processing*, pp. 425–464, 2010.

[14] M. Paipuri, L. Leclercq, and J. Krug, "Validation of macroscopic fundamental diagrams-based models with microscopic simulations on real networks: Importance of production hysteresis and trip lengths estimation," *Transportation Research Record*, vol. 2673, pp. 478–492, 2019.

[15] H. Zhou, H. Kong, L. Wei, D. Creighton, and S. Nahavandi, "Efficient road detection and tracking for unmanned aerial vehicle," *IEEE Transactions on Intelligent Transportation Systems*, vol. 16, pp. 297–309, 2015.

[16] E. N. Barmpounakis, E. I. Vlahogianni, and J. C. Golias, "Unmanned aerial aircraft systems for transportation engineering: current practise and future challenges," *International Journal of Transportation Science and Technology*, vol. 5, pp. 111–122, 2016.

[17] S. Wang, F. Jiang, B. Zhang, R. Ma, and Q. Hao, "Development of UAV-based target tracking and recognition systems," *IEEE Transactions on Intelligent Transportation Systems*, pp. 3409–3422, 2020.

[18] Y. Englezou, S. Timotheou, and C. G. Panayiotou, "Estimating the Origin-Destination matrix using link count observations from Unmanned Aerial Vehicles," *2021 IEEE International Intelligent Transportation Systems Conference (ITSC)*, pp. 3539–3544, 2021.

[19] E. Barmpounakis and N. Geroliminis, "On the new era of urban traffic monitoring with massive drone data: the pNEUMA large-scale field experiment," *Transportation Research Part C*, pp. 50–71, 2020.

[20] Y. Englezou, S. Timotheou, and C. G. Panayiotou, "Probabilistic traffic density estimation using measurements from unmanned aerial vehicles," *IEEE International Conference on Unmanned Aircraft Systems*, 2022.

[21] L. Edie, "Discussion of traffic stream measurements and definitions," *Proceedings of the 2nd International Symposium on the Theory of Traffic Flow*, pp. 139–154, 1963.

[22] M. Sederlin, X. Ma, and J. Jin, "A hybrid modelling approach for traffic state estimation at signalized intersections," *IEEE Intelligent Transportation Systems Conference (ITSC)*, pp. 3604–3609, 2021.

[23] S. Banerjee, B. Carlin, and A. Gelfand, *Hierarchical Modeling and Analysis for Spatial Data*, 2nd ed. Boca Raton: Chapman and Hall/CRC, 2004.

[24] P. A. Lopez, M. Behrisch, L. Bieker-Walz, J. Erdmann, Y.-P. Flötteröd, R. Hilbrich, L. Lücken, J. Rummel, P. Wagner, and E. Wiebner, "Microscopic traffic simulation using SUMO," *Proceedings of the 21st IEEE International Conference on Intelligent Transportation Systems (ITSC)*, pp. 2575–2582, 2018.

[25] J. P. Chilés and N. Desassis, *Handbook of Mathematical Geosciences*. Springer, 2018, ch. Fifty Years of Kriging.